Journal of Power Sources 195 (2010) 2623–2627

Contents lists available at ScienceDirect

Journal of Power Sources

journal homepage: www.elsevier.com/locate/jpowsour

Short communication

Effect of heat-treatment temperature on carbon corrosion in polymer electrolyte membrane fuel cells

Young-Jin Ko, Hyung-Suk Oh, Hansung Kim*

Dept. of Chemical and Biomolecular Engineering, Yonsei University, 134 Shinchon-Dong, Seodaemun-gu, 120-749 Seoul, Republic of Korea

ARTICLE INFO

Article history:
Received 28 July 2009
Received in revised form
18 September 2009
Accepted 5 November 2009
Available online 24 November 2009

Keywords:
Carbon nanofiber
Durability
Heat-treatment temperature
Carbon corrosion
Polymer electrolyte membrane fuel cell

ABSTRACT

This study examines the effect of heat-treatment temperature on the electrochemical corrosion of carbon nanofibers (CNFs) in polymer electrolyte membrane (PEM) fuel cells. Corrosion is investigated by monitoring the generation of CO_2 using an on-line mass spectrometer at a constant potential of 1.4 V for 30 min. The experimental results show that the generation of CO_2 decreases with increasing heat-treatment temperature, indicating that less electrochemical carbon corrosion occurs. In particular, when the heat-treatment temperature is 2400 °C, the change intensifies. X-ray photoelectron spectroscopic analysis shows that oxygen functional groups on the carbon surface decrease with increasing heat-treatment temperature. A reduction in oxygen functional groups increases the hydrophobic nature of the carbon surface, which is responsible for the increased corrosion resistance of CNFs.

1. Introduction

In recent years, electrochemical corrosion of carbon in the catalyst layers of polymer electrolyte membrane fuel cells (PEMFCs) has received much attention because the corrosion process is a critical factor in limiting cell durability [1–3]. At present, carbon-based materials are adapted for catalyst supports in PEMFCs, but carbon is thermodynamically unstable under the normal operating conditions. The equilibrium potential for carbon oxidation to carbon dioxide is 0.207 V vs. SHE at 25 °C [4]. Although thermodynamically unstable, slow kinetics allow the use of carbon in PEMFCs; under normal operating conditions, the extent of carbon corrosion is small. On the other hand, the corrosion rate increases notably during iterative abnormal reverse-current conditions [5,6]. When carbon is corroded, Pt particles aggregate and this results in a decrease in the active surface area of the Pt catalyst. Thus, using carbon catalyst supports that are vulnerable to carbon corrosion leads to rapid degradation of PEMFC performance [7].

Various carbon materials have been tested as supports for Pt catalysts. Typically, carbon black (CB) is the most frequently employed support material, although it has been reported that CB undergoes serious intrinsic corrosion under abnormal operating conditions. The problems intrinsic to the use of CB in PEMFCs have stimulated a search for alternative carbon supports, such as carbon nanotubes (CNTs), carbon nanofibres (CNFs), and carbon nanocages (CNCs), because it is well known that a high degree of graphitization favours an increase in corrosion resistance [8–11]. Aside from graphitization of the carbon support, our previous investigations showed that the hydrophobicity of a carbon surface also plays an important role in decreasing carbon corrosion [12,13].

This study explores the benefits of heat treatment on CNF supports, as a pretreatment process, to suppress carbon corrosion. This approach is motivated by the fact that heat-treatment appears to produce hydrophobic carbon surfaces by eliminating oxygen functional groups on the surface. Higher heat-treatment temperatures can increase processing costs; hence the correlation between the degree of carbon corrosion and heating temperature is quantified to find the minimum temperature required to achieve corrosion resistance. On-line mass spectrometry, which has been introduced in a previous report, was used to measure the carbon corrosion by monitoring the quantity of CO_2 emitted during electrochemical oxidation [7], because the generation of CO_2 provides direct evidence of carbon corrosion.

2. Experimental

Pt/CNF catalysts (from Suntel Co. Ltd.) were chosen to study the effects of heat-treatment temperature. Pt/C catalysts from Johnson Matthey Co. (40 wt.% Pt) were used for the anode, and Pt/CNF samples for the cathode catalyst, to compare carbon corrosion behaviour. The CNF samples that were untreated, heat-treated at 1600, 2000, 2400, and 2800 °C are denoted as G-raw, G-16, G-

* Corresponding author. Tel.: +82 2 2123 5753; fax: +82 2 312 6401.
E-mail address: elchem@yonsei.ac.kr (H. Kim).

0378-7753/$ – see front matter © 2009 Elsevier B.V. All rights reserved.
doi:10.1016/j.jpowsour.2009.11.071

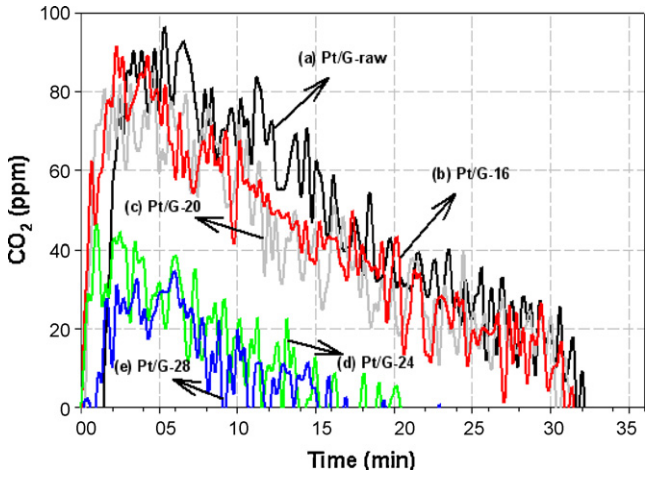

Fig. 1. Comparison of CO_2 mass spectra profiles for MEAs at 1.4 V for 30 min. (a) Pt/G-raw, (b) Pt/G-16, (c) Pt/G-20, (d) Pt/G-24, and (e) Pt/G-28.

20, G-24 and G-28, respectively. The anode and cathode catalyst inks were prepared by ultrasonically blending each catalyst with Nafion solution (5 wt.%) and isopropyl alcohol. The catalyst inks were then sprayed on to a Nafion 212 membrane to prepare membrane electrode assemblies (MEAs). Testing of PEMFC durability was performed on a fuel cell with a 5 cm^2 active surface area, and with a catalyst loading 0.4 mg cm^{-2} at both the anode and the cathode.

Several electrochemical experiments were carried out before and after corrosion tests to examine the physical and electrochemical changes associated with carbon corrosion. To plot the polarization curve, the cells were conditioned with 150 ccm flow rates of H_2(anode) and O_2(cathode) at 75 °C under atmospheric pressure. Impedance tests were conducted at 0.8 V to measure the membrane and charge-transfer resistance. After completion of the impedance analysis, cyclic voltammetry (CV) experiments were performed to determine the electrochemically active surface area of the catalysts. A scan rate of 50 mV s^{-1} was used to sweep the working electrode from 0.05 to 1.2 V vs. the anode. To test the corrosion of the carbon support, a constant potential of 1.4 V against

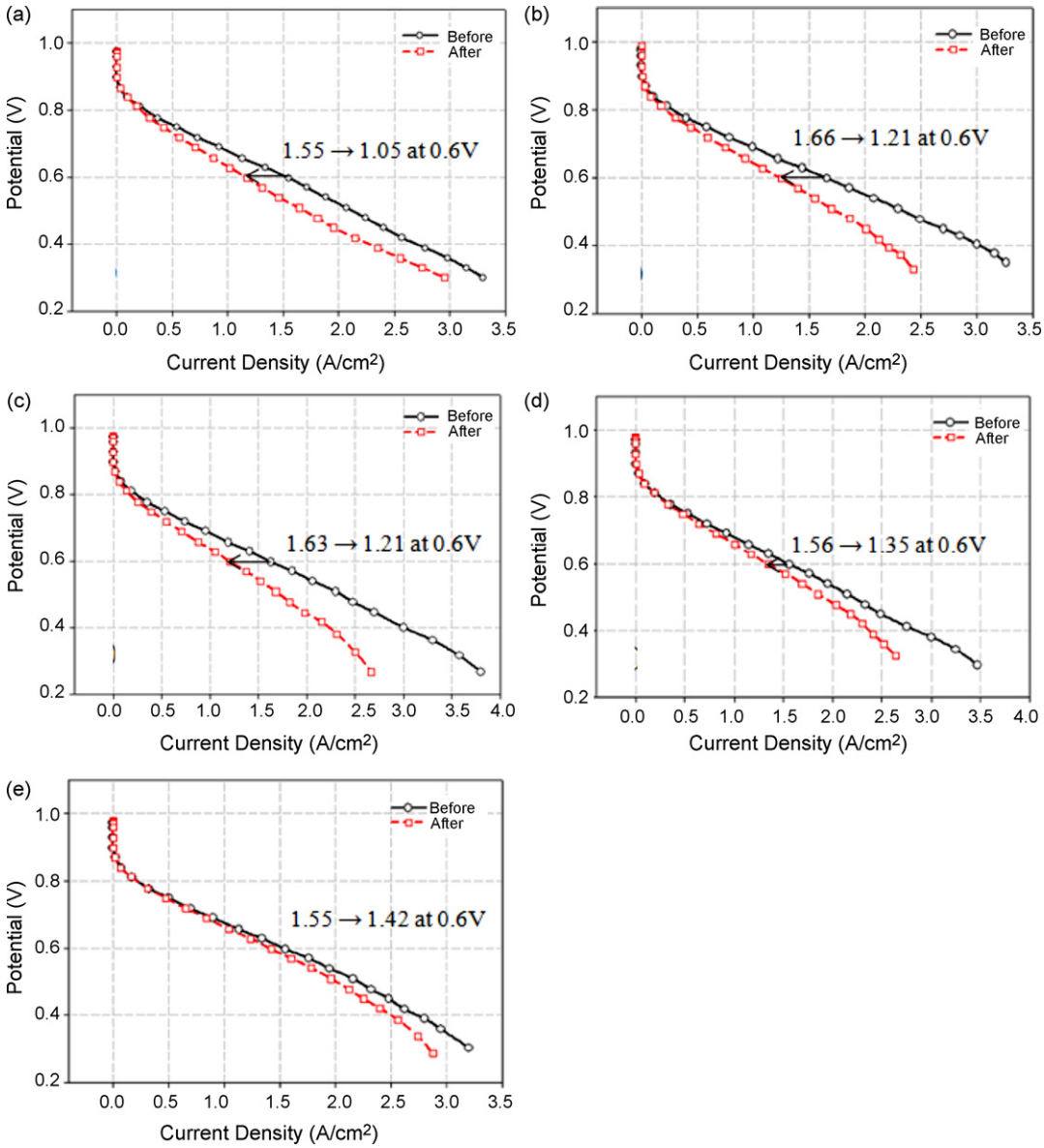

Fig. 2. Polarization curves of MEAs before and after corrosion tests with respect to CNF heat-treatment temperatures. (a) Pt/G-raw, (b) Pt/G-16, (c) Pt/G-20, (d) Pt/G-24, and (e) Pt/G-28.

the anode was applied for 30 min. The anode of the fuel cell was exposed to fully humidified H_2 at 20 ccm, and the cathode of the fuel cell was exposed to fully humidified N_2 at 30 ccm. The cell and humidifier temperatures were fixed at 90 °C. The cathode was connected to a mass spectrometer, and the amount of CO_2 produced at the cathode was monitored with respect to time.

X-ray diffraction (XRD) studies were performed to inspect the graphitic structure of CNFs and to calculate the Pt particle size. The ratio and the types of functional group on the surfaces of carbon supports were characterized by X-ray photoelectron spectroscopy (XPS). Inductively coupled plasma atomic emission spectroscopy (ICP–AES) analysis was conducted to estimate the Pt loading over the carbon support.

The specific surface area of CNFs was measured by means of the Brunauer, Emmet, Teller (BET) method. The double-layer charge of CNFs caused by an increase in heat-treatment temperature was investigated under half-cell conditions using 0.5 M H_2SO_4 as the electrolyte. Cyclic voltammogram (CV) experiments were conducted between 0.04 and 1.04 V (vs. SHE) using a bi-potentiostat (CH instruments). Dispersion of heat-treated CNFs in water was carried out in order to confirm their hydrophobicity. One milligram of each CNF was wetted with 15 mL water and dispersed by sonication. The mixtures were then agitated swiftly by hand and observed for changes.

3. Result and discussion

3.1. Corrosion investigation of Pt/CNF samples

Corrosion tests were conducted by applying a Pt/CNF catalyst at the cathode. Fig. 1 shows a mass spectrogram that indicates CO_2 formation during the corrosion tests. These tests were conducted using carbon supports that had each been subjected to different heat-treatment temperatures. A comparison of CO_2 generation from the five samples shows that G-raw yields the greatest CO_2 production. The generation of CO_2 tends to decrease with increasing heat-treatment temperature, and a considerable decrease is observed for the G-24 sample. This implies that the heat treatment of CNF plays a critical role in increasing the resistance to carbon corrosion, and temperature higher than 2400 °C is required for a noticeable reduction in carbon corrosion.

The performance of the MEAs in fuel cells was evaluated; the results are shown in Fig. 2. As the heat-treatment temperature increases, the ratio of performance loss decreases. As shown in Fig. 1, the MEAs with smaller performance reductions show less production of CO_2. As expected from mass spectrometry, a major change in performance loss is detected at 2400 °C. The untreated samples (G-raw) experience a 32% decrease in performance at 0.6 V whereas G-16, G-20, G-24 and G-28 suffer 27.1, 25.8, 11.5 and 8.4% decreases, respectively.

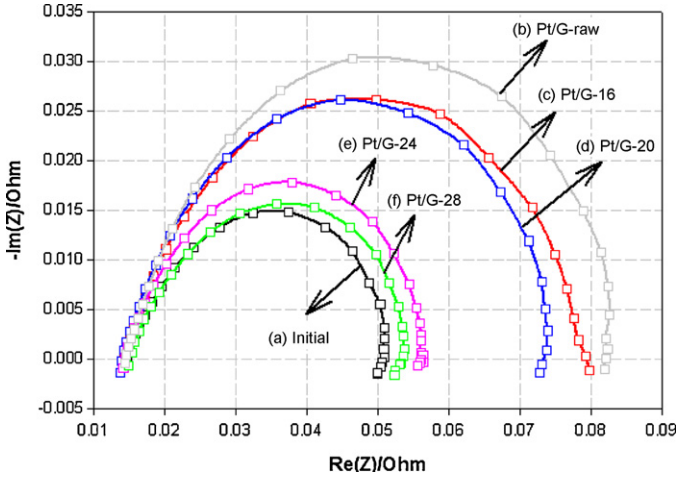

Fig. 3. Nyquist plots of MEAs at 0.8 V before and after corrosion tests. (a) Initial, (b) Pt/G-raw, (c) Pt/G-16, (d) Pt/G-20, (e) Pt/G-24, and (f) Pt/G-28.

Table 2
BET surface areas of CNFs with different heat-treatment temperatures.

Sample	BET surface area ($m^2\ g^{-1}$)
G-raw	75.2100
G-16	54.1177
G-20	49.4519
G-24	49.2073
G-28	48.8753

The initial and final impedances of each sample are presented in Fig. 3. The membrane resistance shows no distinctive difference between the samples and does not change after the corrosion test. By contrast, the charge-transfer resistance decreases with increasing heat-treatment temperature. Similarly, notable differences are observed at 2400 °C. To examine the changes in the active Pt surface area, CV measurements on MEAs were conducted before and after corrosion tests. As indicated in Table 1, carbon corrosion is responsible for a severe decrease in the active surface area. A lower degree of carbon corrosion, as measured by mass spectrometry, yields smaller changes in the active Pt surface area.

3.2. Characterization of heat-treated carbons

Table 2 shows the BET surface area of five CNF samples treated at different temperatures. According to BET analysis, the untreated

Table 1
Summary of changes before and after corrosion tests for Pt/CNF catalysts.

Condition	MEA performance at 0.6 V ($A\ cm^{-2}$)		Active surface area ($m^2\ g^{-1}$)		Membrane resistance		Charge-transfer resistance		Mass data (μL)
	Before	After	Before	After	Before	After	Before	After	30 min at 1.4 V
(G-raw) Pt/Raw CNF	1.55	1.05	38.7	31	0.0147	0.0148	0.0347	0.0668	53 μL
	−32%	−20%	+0%	+92.5%					
(G-16)Pt/1600 °C heat-treated CNF	1.66	1.21	32.7	26.7	0.014	0.0142	0.0348	0.0655	38 μL
	−27.1%	−18.3%	+1.4%	+88.2%					
(G-20)Pt/2000 °C heat-treated CNF	1.63	1.21	29.3	23.9	0.014	0.014	0.0352	0.0591	40 μL
	−25.8%	−18.4%	0%	+67.9%					
(G-24)Pt/2400 °C heat-treated CNF	1.56	1.38	27.4	24.5	0.0143	0.0143	0.0367	0.0422	10 μL
	−11.5%	−10.6%	0%	+15.0%					
(G-28)Pt/2800 °C heat-treated CNF	1.55	1.42	25.0	23.2	0.0149	0.0149	0.0368	0.0383	7 μL
	−8.4%	−7.2%	0%	+4.1%					

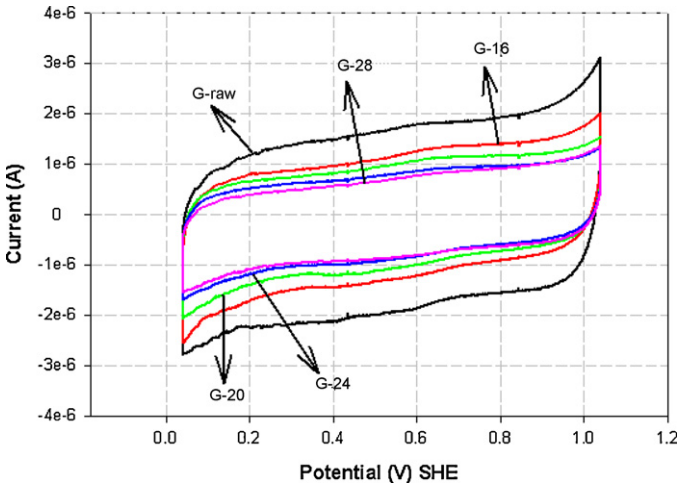

Fig. 4. Cyclic voltammograms of CNFs obtained in 0.5 M H_2SO_4. CV of untreated CNF is also displayed for comparison. Voltage scan rate 5 mV s^{-1}. (a) Pt/G-raw, (b) Pt/G-16, (c) Pt/G-20, (d) Pt/G-24, and (e) Pt/G-28.

CNF support has a larger BET surface area than heat-treated CNF. In general, BET surface area decreases with increasing heat-treatment temperature. The difference is however, not large.

The CV of each CNF under half-cell conditions is presented in Fig. 4. The double-layer charge of CNFs tends to decrease as the heat-treatment temperature increases. This trend is directly correlated to the BET surface area. Because the double-layer charge is directly proportional to the surface area of the carbon, the largest change is observed between untreated G-raw and G-16. G-24 and G-28, which do not have large differences in BET surface area, do not display much difference in double-layer charge.

Fig. 5 displays the XPS C1s spectrum of G-raw, which allows identification of the oxygen-containing functional groups on the carbon surface. The binding energies of functional groups are assigned to the deconvoluted peaks as follows: sp^2 C=C of aromatic graphite on the CNF structure (BE = 284.3 eV), sp^3 C–C of aliphatic graphite on the CNF structure (BE = 285.1 eV), C–O (BE = 287.6 eV), and C=O (BE = 286.4 eV). The position of the main C1s line at 284.3–284.6 eV indicates that carbon is in the form of graphite [14]. Note that the π–π^* transition loss peak is detected at 290–291 eV in the XPS spectra of CNF, thus demonstrating the presence of a graphitic structure [15]. By integrating the areas under the high-resolution XPS O1s and C1s peaks, followed by corrections using sensitivity factors, the oxygen and carbon ratio (O:C ratio) for each

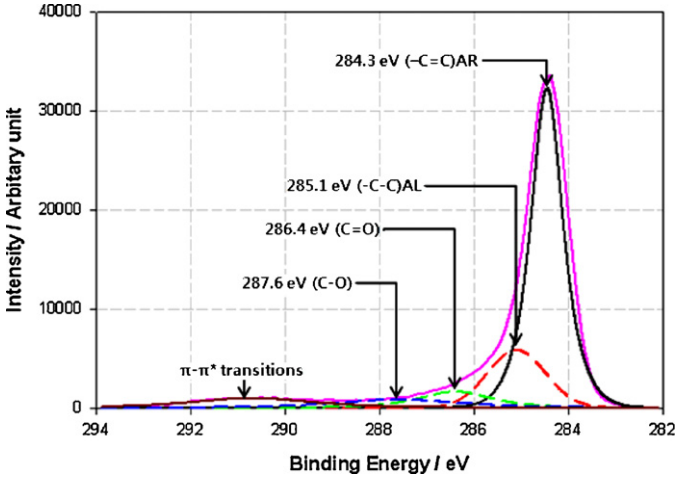

Fig. 5. XPS C1s spectra of untreated CNF (G-raw).

Table 3
The O:C atomic ratios of CNF surfaces obtained by XPS analysis.

Sample	% O	% C
G-raw	2.73	97.27
G-16	1.81	98.19
G-20	1.71	98.29
G-24	1.36	98.64
G-28	0.97	99.03

CNF is calculated [16]. The results listed in Table 3 shows that the amount of oxygen on the carbon surface decreases with increasing heat-treatment temperature, with the effect being particularly pronounced at 1600 and 2400 °C. Based on XPS analysis, it is expected that increasing the heat-treatment temperature results in more hydrophobic CNF surfaces due to a decrease in the oxygen ratio on the carbon surface [17]. This is confirmed by observing dispersions of CNFs in deionized water, as shown in Fig. 6. Initially, the CNF samples are uniformly dispersed in water using an ultrasonic bath. After 24 h, the CNF heat-treated at temperatures higher than 2400 °C sediments by forming large aggregates, where as the CNFs heat-treated at temperatures below 2000 °C are relatively stable. These results demonstrate that heat treatment above 2400 °C changes the carbon surface from hydrophilic to hydrophobic. According to the reported mechanism of carbon corrosion, functional oxygen groups are generated on the carbon surface upon contact with water (Eq. (1)), and are, in turn, converted into CO_2 (Eq. (2)) at a high overpotential [18]:

$$C + H_2O \rightarrow C\text{–}O_{ad} + 2H^+ + 2e^- \quad (1)$$

$$C\text{–}O_{ad} + H_2O \rightarrow CO_2 + 2H^+ + 2e^- \quad (2)$$

It was confirmed in our previous studies that water facilitates electrochemical carbon corrosion in fuel cell systems [12]. Hence, inducing hydrophobic carbon surface by heat treatment may be responsible for enhancing the corrosion resistance of carbon supports.

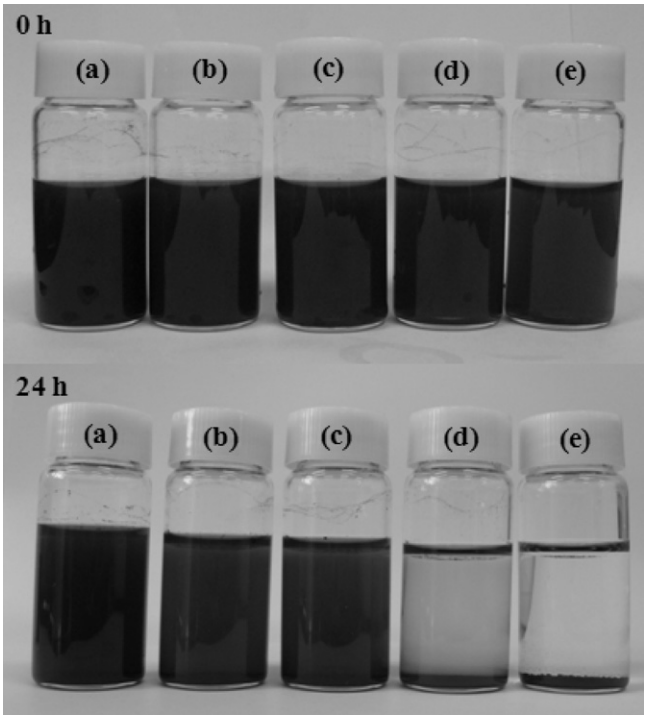

Fig. 6. Dispersion of carbon supports in water at initial time and after 24 h. (a) G-raw, (b) G-16, (c) G-20, (d) G-24, and (e) G-28.

Table 4
Pt content and particle size of Pt supported by different CNFs.

Sample	ICP (wt.%)	Particle size in XRD (nm)
(G-raw)Pt/Raw CNF	36.5	2.9
(G-16)Pt/1600 °C heat-treated CNF	37.2	3.0
(G-20)Pt/2000 °C heat-treated CNF	37.2	3.0
(G-24)Pt/2400 °C heat-treated CNF	37.9	3.2
(G-28)Pt/2800 °C heat-treated CNF	37.4	3.3

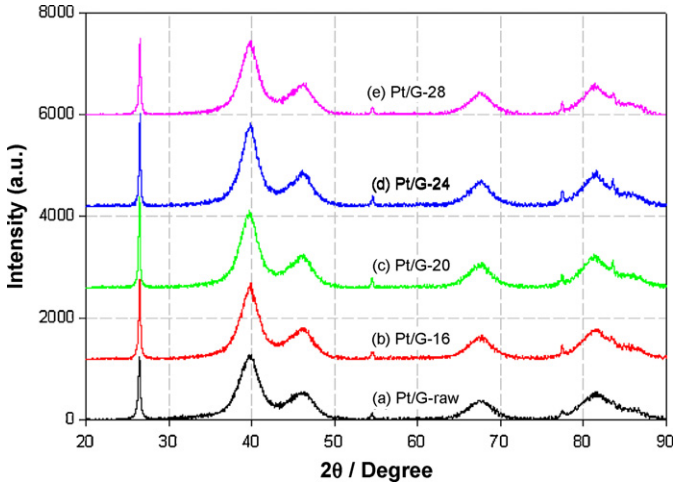

Fig. 7. XRD patterns of Pt particles on CNF that has been subjected to different heat-treatment temperatures. (a) Pt/G-raw, (b) Pt/G-16, (c) Pt/G-20, (d) Pt/G-24, and (e) Pt/G-28.

3.3. Characterization of Pt/CNF samples

Table 4 presents the physical properties of Pt-supported CNF samples. According to ICP analysis, the wt.% of platinum in the five samples is similar. The particle size of platinum and the degree of graphitization of the CNFs are confirmed by the XRD patterns shown in Fig. 7. The mean particle sizes are calculated from Scherrer's formula based on the Pt (2 2 0) peak. As the CNF heat-treatment temperature is increased, the size of the Pt particles loaded on CNF increases. A strong and narrow diffraction peak (0 0 2) is observed at $2\theta = 26.2^\circ$. This peak is attributed to the graphitic structure of the CNF supports. From this (0 0 2) peak, the crystallite thickness (L_c value) and the interlayer spacing (d_{002} value) are calculated using Scherrer's formula and Bragg's law. A higher L_c value for the (0 0 2) peak and a lower d_{002} number imply increased graphitization [19–21]. However, the XRD patterns show that a significant shift of the (0 0 2) peak is not detected in the heat-treated CNF samples. This indicates that an increase in heat-treatment temperature does not significantly influence the degree of graphitization. Thus, an increase in resistance to electrochemical carbon corrosion does not originate from an increase of graphitization, but from an increase in the hydrophobicity of the carbon surfaces.

4. Conclusions

An evaluation has been made of the electrochemical carbon corrosion of Pt/CNF, in which the CNFs were treated at different temperatures. The BET surface area decreases as the heat-treatment temperature is increased, leading to an increase in the size of the particles. An increase in heat-treatment temperature endows CNFs with more resistance to electrochemical carbon corrosion. In particular, when the heat-treatment temperature reaches 2400 °C, the change becomes noticeable. As the heat-treatment temperature is increased, the oxygen ratio on the carbon surface decreases, while the degree of graphitization on CNF does not change significantly. Therefore, an increase in hydrophobicity, arising from a decreased ratio of surface-bound oxygen produced by the heat-treatment process, is considered to be responsible for the increase in corrosion resistance.

Acknowledgment

This work was supported by the New & Renewable Energy R&D program (2009T100100606) under the Ministry of Knowledge Economy of Korea, and the National Research Foundation (NRF-2009-0092926) of Korea Grant funded by the Korean Government (MEST). We thank Suntel Co. Ltd. for providing catalysts.

References

[1] E. Antolini, J. Mater. Sci. 38 (2003) 2995–3005.
[2] X. Cheng, L. Chen, C. Peng, Z.W. Chen, Y. Zhang, Q.B. Fan, J. Electrochem. Soc. 151 (2004) A48–A52.
[3] J. Willsau, J. Heitbaum, J. Electroanal. Chem. 161 (1984) 93–101.
[4] Y. Shao, G. Yin, Y. Gao, J. Power Sources 171 (2007) 558–566.
[5] C.A. Reiser, L. Bregoli, T.W. Patterson, J.S. Yi, J.D. Yang, M.L. Perry, T.D. Jarvi, Electrochem. Solid-State Lett. 8 (2005) A273–A276.
[6] H. Tang, Z. Qi, M. Ramani, J.F. Elter, J. Power Sources 158 (2006) 1306–1312.
[7] H.S. Oh, J.G. Oh, S. Haam, K. Arunabha, B. Roh, I. Hwang, H. Kim, Electrochem. Commun. 10 (2008) 1048–1051.
[8] K.H. Lim, H.S. Oh, H. Kim, Electrochem. Commun. 11 (2009) 1131–1134.
[9] X. Wang, W. Li, Z. Chen, M. Waje, Y. Yan, J. Power Sources 158 (2006) 154–159.
[10] L. Li, Y. Xing, J. Electrochem. Soc. 153 (2006) A1823–A1828.
[11] Y. Shao, G. Yin, J. Zhang, Y. Gao, Electrochim. Acta 51 (2006) 5853–5857.
[12] K.H. Lim, H.S. Oh, S.E. Jang, Y.J. Ko, H.J. Kim, H. Kim, J. Power Sources 193 (2009) 575–579.
[13] H.S. Oh, K.H. Lim, B. Roh, I. Hwang, H. Kim, Electrochim. Acta 54 (2009) 6515–6521.
[14] J.R. Pels, F. Kapteijn, J.A. Moulijn, Q. Zhu, K.M. Thomas, Carbon 33 (1995) 1641–1653.
[15] K.H. Kangasniemi, D.A. Condit, T.D. Jarvi, J. Electrochem. Soc. 151 (2004) E125–E132.
[16] T.C. Kuo, A. McCreery, Anal. Chem. 71 (1999) 1553–1560.
[17] H. Shengliang, B. Peikang, T. Fei, C. Shirui, S. Jing, Carbon 47 (2009) 876–883.
[18] S. Maass, F. Finsterwalder, G. Frank, R. Hartmann, C. Merten, J. Power Sources 176 (2008) 444–451.
[19] T.H. Hyeon, S.J. Han, Y.E. Sung, K.W. Park, Y.W. Kim, Angew Chem. Int. Ed. 42 (2003) 4352–4356.
[20] Y.A. Zhu, Zh.J. Sui, T.J. Zhao, Y.Ch. Dai, Zh.M. Cheng, W.K. Yuan, Carbon 43 (2005) 1694–1699.
[21] K. Kinoshita, Carbon: Electrochemical and Physicochemical Properties, John Wiley & Sons, 1998.